Russian Geology and Geophysics © 2020, V.S. Sobolev IGM, Siberian Branch of the RAS
Vol. 61, No. 8, pp. 917–928, 2020 *DOI:10.15372/RGG2019186* *Geologiya i Geofizika*

Extension of the Dynamic Range of Laterolog Tools by Digital Signal Processing

V.A. Klimenko[a, ✉], T.R. Salakhov[a], V.M. Korovin[b]

[a] *AO NPF Geofizika, ul. Komsomolskaya 2, Ufa, 450513, Russia*

[b] *AO Bashneftegeofizika, ul. Lenina 13, Ufa, 450077, Russia*

Received 17 October 2018; received in revised form 2 May 2019; accepted 27 November 2019

Abstract—We consider the ranges of current and voltage values for laterolog tools. It is shown that expansion of the dynamic range of these parameters is possible by mathematical focusing and digital filtering and by fulfillment of the conditions for the effective number of bits and by compliance with the tool requirements. The principles of mathematical focusing are considered by the example of the 5BK tool designed by AO NPF Geofizika (Joint-Stock Company) in Ufa. The digital-filtering calculation and application technique is described. The results of well tests are presented.

Keywords: electric logging, lateral logging, laterolog tool, dynamic range, mathematical focusing, digital signal processing, digital filtering, well effect

INTRODUCTION

In connection with beginning of development of the offshore oil and gas deposits in Russia and conducting exploratory drilling with large borehole diameters, as well as using highly mineralized drilling muds, new requirements for geophysical tools that measure electrical resistivity of rocks are emerging. Induction tools do not work under these conditions. The main method for determining electrical resistivity of layers in water-based mud is the Laterolog. Laterolog tools reach saturation under these conditions too early, that is, they underestimate readings due to the strong influence of the borehole, which is not corrected by charts. Thus, the purpose of this study was to explore the ways of extending the dynamic range of the laterolog tools.

For electrical (galvanic) logging tools, the ratio of the measured voltage (or combination of measured voltage) to the generated current (or combination of currents) multiplied by the coefficient of the sonde is called apparent resistivity:

$$\rho_k = K_s \cdot \frac{U_{NNy}}{I_0}, \quad (1)$$

where K_s is coefficient of the sonde, U_{NNy} is the measured voltage, I_0 is the generated current (Il'inskii, 1971; Dakhnov, 1981).

Considering equation (1) for galvanic tools in general, the dynamic range of measurement is determined by the accuracy of current and voltage measurements (a combination of current and voltage measurements) (Itskovich et al., 1998; Smith et al., 1998; Legendre et al., 1999; Zhou et al., 2008; Maurer et al., 2009; Khusid et al., 2014; Kayurov et al., 2015). In practice, the current is often set constant and independent of the load resistance. Because of this, the voltage change on the measuring electrodes has a large dynamic range and therefore has a very small value in high-resistivity layers.

WAYS TO INCREASE THE DYNAMIC RANGE. MATHEMATICAL FORMULATION

For the tool with the 5LL sonde (in Russian transcription 5BK, more information can be found in references (Klimenko et al., 2019; Salnikova et al., 2019)), that is produced in Geofizika Joint-Stock Company (Ufa), modeling and research of the metrological characteristics was carried out. This modeling includes the dynamic range of the voltage changing between the electrodes *MN* (U_{MN}^{AiAi+1}) and *NNy* (U_{NNy}^{AiAi+1}), when root-mean-square (RMS) current value equals to 1 A on the generating electrodes. The dynamic range was determined by a combination of possible electrical parameters: formation resistivity, mud resistivity and the borehole diameter. The simulation results are shown in Table 1. The voltage between the measuring electrodes *N* and *Ny* varies in the range from a few millivolts up to units of volts, which is an acceptable signal level for measurement. The voltage between the electrodes *M* and *N* can vary from units of microvolts to hundreds of millivolts, so it is a difficult task to ensure good measurement of such signals, since these signals are superimposed with a variety of noise and interference. Based on the experience of designing of galvanic tools, the noise level can reach levels of tens of milli-

✉ Corresponding author.
E-mail address: KlimenkoVA@npf-geofizika.ru (V.A. Klimenko)

Table 1. Dynamic range of measured voltages

Voltage between *M* and *N* electrodes in the corresponding mode	U_{min}, mV	U_{max}, mV	Voltage between *N* and *Ny* electrodes in the corresponding mode	U_{min}, mV	U_{max}, mV
U_{MN}^{A0A2}	30	1000	U_{NNy}^{A0A2}	30	2500
U_{MN}^{A1A2}	0.015	200	U_{NNy}^{A1A2}	12	3000
U_{MN}^{A2A3}	0.006	120	U_{NNy}^{A2A3}	12	3000
U_{MN}^{A3A4}	0.006	90	U_{NNy}^{A3A4}	10	3000
U_{MN}^{A4A5}	0.006	60	U_{NNy}^{A4A5}	8	3000
U_{MN}^{A5A6}	0.006	60	U_{NNy}^{A5A6}	8	3000

volts. In this case, the noise level may exceed the useful signal by a factor of 10,000 (80 dB) or more.

One of the ways to raise the level of the measured signals is to increase the power "pumped" into the formation. However, this leads to an increase in the total power consumption, as well as, generally, to a decrease in the efficiency (for linear amplifiers of classes A, B, AB and similar amplifiers (Gusev, 2013)). This is not always acceptable. Moreover, doubling the output current leads only to a proportional double increase in the voltage on the measuring electrodes, while it does not solve the problem of the low signal level.

Analog filtration may be used to reduce the noise level in the measured signals, but the maximum possible suppression coefficient is only 60–70 dB/Dec (Kajazkas, 1988). This limit is caused by the intrinsic noise of the operational amplifiers and passive components. In addition, the filter must be of a high order due to the proximity of the measured signal and the main noise in the spectrum. Therefore, the measurement of this level of signals is possible by using digital signal processing (DSP), and in particular, digital filtration (DF).

The use of DSP is necessary, but there are other requirements for laterolog tools, non-compliance with which leads to futility of any DSP.

Firstly, a mandatory requirement is the use of mathematical (numerical) focusing for laterolog tools, which allows avoiding hardware restrictions (the finite resistances of "shunts" and "short circuits" between the electrodes inside the tool).

Consider the principle of mathematical focusing on the example of the 5LL tool (AO NPF Geofizika, Ufa). Figure 1 shows the distribution scheme of the current lines for all the different dipoles of the electrodes A0-A2, A1-A2, A2-A3, A3-A4, A4-A5, A5-A6. The position of the remote electrode *Ny* is displayed not to scale. Also, in the figure, voltmeters V1 and V2 show which voltages are measured at the corresponding dipole. Different depth of investigation achieved by alternately turning on and remoting the dipoles from the measuring electrodes *M* and *N*. Due to the constant distance between the measuring electrodes *M* and *N*, a single vertical resolution is provided for each sonde. The vertical resolution is the length between the midpoints of the measuring electrodes *M* and *N* on each side of the center of the instrument, and is 0.38 m. The depth of the investigation depends on the borehole conditions and the pseudogeometric factor and is approximately 0.2–0.3 m for a shallow and up to 1–1.5 m for a deep sonde (Klimenko et al., 2019).

The system of equations describing the operation of laterolog tools in general can be represented as:

$$\begin{cases} \rho_k = K_s \cdot \dfrac{U_{NNy}}{I_0}; \\ U_{MN} = 0, \end{cases} \tag{2}$$

where K_s is sonde coefficient, U_{NNy} is the voltage between the measuring electrode and the remote electrode, I_0 is the generated current, U_{MN} is voltage between the measuring electrodes.

Mathematical focusing is carried out on the basis of two sequential activations of the dipoles for each sonde. For example, dipoles A0-A2 and A1-A2 are necessary to obtain the apparent resistance (AR) of the first (shallowest) sonde (ρ_{k1}). The measured parameters obtained in the dipole A0-A2 will be used in the future to obtain the readings of the other sondes. At the moment of turning on dipole A0-A2 (the first mode), the voltages U_{NNy}^{A0A2}, U_{MN}^{A0A2} and current I_0 are measured. When turning on dipole A1-A2 (the second mode) voltages U_{NNy}^{A1A2}, U_{MN}^{A1A2} are measured.

Applying the principle of superposition of electrical fields, we assume that the resulting voltage U_{NNy} is the sum of the voltages in the first and second modes, taken with weight coefficients. Taking the weight coefficient for the first dipole equal to one we get:

$$U_{NNy} = U_{NNy}^{A0A2} + K1 \cdot U_{NNy}^{A1A2}, \tag{3}$$

substituting (3) in the first equation of the system (2), we get:

$$\rho_k = K_s \cdot \left(\frac{U_{NNy}^{A0A2} + K1 \cdot U_{NNy}^{A1A2}}{I_0} \right), \tag{4}$$

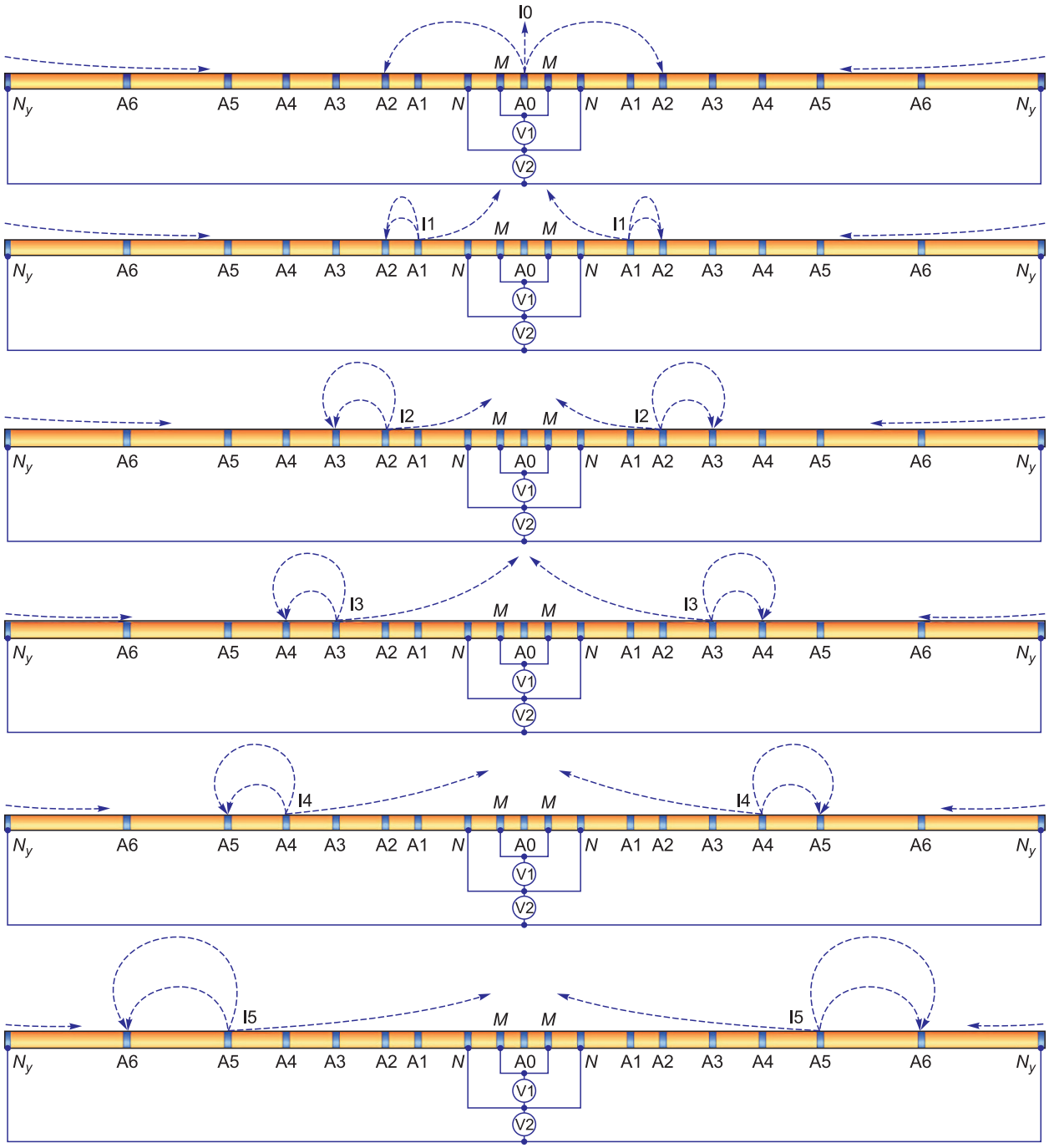

Fig. 1. Modes (dipoles): A0-A2, A1-A2, A2-A3, A3-A4, A4-A5, A5-A6 (top to bottom).

On the other side, the resulting voltage U_{MN} is also the sum of the voltages at the first and second modes and taken with the same weight coefficients as the voltage U_{NNy}^{A0A2} and U_{NNy}^{A1A2}. To ensure focusing, the sum of these voltages must be zero due to the second equation of the system (2):

$$U_{MN} = U_{MN}^{A0A2} - K1 \cdot U_{MN}^{A1A2} = 0. \quad (5)$$

The minus sign in equation (5) appears due to the fact that the voltages (between M and N) in the mode of the first and second dipole, were multidirectional.

$$K1 = \frac{U_{MN}^{A0A2}}{U_{MN}^{A1A2}}. \quad (6)$$

Substituting (6) in (4), we get the equation of apparent resistivity for the first sonde from the measurements of the first and second modes:

$$\rho_{k1} = K_s 1 \cdot \frac{\left(U_{NNy}^{A0A2} + \frac{U_{MN}^{A0A2}}{U_{MN}^{A1A2}} \cdot U_{NNy}^{A1A2} \right)}{I_0}. \quad (7)$$

Similar equations can be derived for the other four sondes. The use of mathematical focusing can significantly simplify the implementation of laterolog tools and reduce the energy spent on current generation.

The measurement errors of each channel are uncorrelated random errors, so the total error of the resistivity will be determined as the average geometric error included in the resistivity equation:

$$\partial\rho_{ki} = \sqrt{\partial I_0^2 + \partial U_{NNy}^2 + \partial U_{MN}^2}, \quad (8)$$

where ∂I_0, ∂U_{NNy}, ∂U_{MN} – relative errors of the measuring channels of tool 5LL. These errors are selected from the maximum channel measurement errors for control points corresponding to the measured resistivity ranges.

Secondly, another mandatory requirement is the bit depth of the used analog-to-digital converter (ADC). If the maximum ADC code is 32,767 bits (a sixteen-bit sign ADC), and the minimum ADC code is 4 (the beats of the two lower ADC bits), then the maximum suppression coefficient that can be implemented using this ADC is calculated as K_{sc} = 4/32767, which in the logarithmic form is 78.3 dB. Table 2 shows the approximate maximum possible suppression coefficients for different ADC resolutions.

According to Table 2, ADCs with the bit depth of less than 15 are not suitable for the use of digital filtering, since they will not be able to provide the desired suppression coefficient, and a low signal level will simply "drown" in noise. The ADC bit depth of 15 is at the limit when digital filtering still makes sense. It is desirable to use an ADC with the bit depth of 15 or higher, but the upper value of the bit depth is also limited by the conversion rate.

Thirdly, there are certain requirements to make measurement circuits more resistant to interference and noise at the level of hardware. Here is the list of the main requirements:
– for analog amplification and filtration paths, highly stable operational amplifiers should be used with a low level of intrinsic noise, a small drift of output voltages from temperature, and a large power supply ripple rejection ratio;
– for analog amplification and filtering paths, it is necessary to use highly stable passive components such as NP0 (C0G) capacitors;
– it is desirable to use linear power supplies, because of their low output noise level and the absence of switching elements (Klaassen, 1996).

Table 2. Suppression ratio

ADC bit depth	Maximum code	Suppression coefficient, dB
12	4095	–60.2
13	8191	–66.2
14	16,383	–72.2
15	32,767	–78.3
16	65,535	–84.3
17	13,1071	–90.3
18	262,143	–96.3

It should be noted that the intrinsic interference induced by the current generator in the formation on the measuring circuits cannot be separated from the true measured signal using digital filtration. In galvanic logging tools, the parasitic signal from the generator to the measuring circuits coincides in frequency and is in the same phase with the measured signal due to the use of low frequencies (there is no phase shift). Because of this, there are no digital filtration criteria for finding this interference. The hardware methods for dealing with such interference are:
– placing the measuring PCB boards (operational amplifiers, analog filters, ADCs) as close to the measuring electrodes as possible (based on the author's personal experience, placement of the measuring boards from the electrodes at a distance of 5 cm allowed reduction of the "generator" interference by about 20 times compared to 1 m);
– for measuring paths, the use of shielded twisted pairs, as well as their placement as far as possible from the generating circuits (laying the measuring and generating wires in different harnesses on different sides of the tool, based on the author's personal experience, allowed reduction of the "generator" interference by about 2 times).

APPLYING AND USE OF DIGITAL FILTRATION

The most important point in any DSP task is to understand how information is entered into the signal to be worked with (Smith, 1999). For geophysical instruments, time domain signals are mostly present at the DSP input. This is because signals are usually generated by samples at regular intervals. However, due to the specific operation of galvanic tools, the required information is located in the frequency domain – in the amplitude of the sine wave, and therefore it is necessary to use digital filtration in the frequency domain.

Here are the necessary parameters for a digital filter that should:
– be band passing;
– have a narrow bandwidth tuned to the frequency of generation;
– have a sharp drop in the amplitude-frequency response in the stopband;
– have a strong rejection ratio in the stopband (preferably more than 80 dB at the main interference frequencies);
– not have signal magnitude changes in the bandwidth;
– work in real time.

The digital filter input receives a discrete input signal $x[n]$, $n = 0 \ldots N-1$. N – is the number of the data samples.

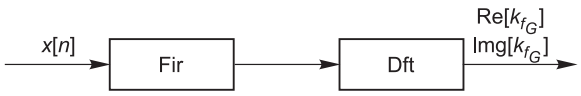

Fig. 2. A block diagram of the digital filter.

For galvanic logging devices, the input signal is created by the ADC before the digital filter from the input analog signal $x(t)$. Each next data sample is received after a time of Δt, i.e., at a sample rate of f_D.

Figure 2 shows the recommended block diagram of a digital filter, which consists of a FIR-filter (finite impulse response) and a DFT module (a discrete Fourier transform).

The length of the impulse response (the filter kernel) of the FIR-filter is assumed to be M, and M must be less than N. Next, the ADC code sample number is iteratively tracked, and when the value $n = M$ is reached, the data are then transferred to the DFT module. The entire range of the measured frequencies is not of interest, so a special case of computing the DFT for a specific harmonic can be used. This computation is a second-order recursive filter (Ifeachor and Jervis, 2001) and computes the complex harmonic amplitude with a certain index k_{fG}, which corresponds to the frequency of generation f_G, reducing the computation time. At the output of the filter, a part of the harmonic of interest is obtained, consisting of the real (Re[k_{f_G}]) and the imaginary part (Img[k_{f_G}]). The magnitude and phase of this harmonic are calculated using the equations for converting a rectangular coordinate system to a polar one.

In order for the scheme to work correctly, one must first suppress all the possible frequency components into a data array, except for the desired one. A FIR-filter was applied in front of the DFT module for this. The disadvantage of using FIR filtering is the need for a large amount of computation, after receiving each subsequent sample. Therefore, the task of designing a FIR-filter consists in achieving the best performance, namely, the maximum rejection ratio and the minimum bandwidth, taking into account all the time limitations that depend on the speed of the microcontroller used and the required logging speed.

The number of the generation periods for digital filtration should be a multiple of the fundamental interference frequencies ("white" noise consisting of all frequencies is neglected). Denote the main interference frequencies by the series $f_0, f_1, f_2, \ldots, f_K$, where K is the maximum interference frequency. In the general case, the generation frequency f_G, can be anywhere between the main interference frequencies. Firstly, the generation frequency f_G should be low enough to correspond to DC models and there should be no phase shift between the signal generated to the formation and the received signal. Secondly, the main interference frequencies and the generation frequency must be multiples of each other, so if f_G is between f_1 and f_2, then the following expression will be true:

$$f_0 \vdots f_1 \vdots f_G \vdots f_2 \ldots \quad (9)$$

If expression (9) is fulfilled, then the interference frequencies will fall into a local minimum at the magnitude frequency response of the digital filter and will have a stronger rejection ratio. In the 5LL tool, the choice of the operating frequency of 250 Hz generation is not accidental. Thus, in the 50 Hz interference frequency, there are 5 periods of the 250 Hz generation frequency or 8 periods of the 400 Hz interference frequency, all the frequencies are multiples of each other. This means that for maximum suppression to be achieved, the observation time must be 5 R periods, where R is a natural number that is determined by the necessary suppression, the required logging speed, the speed of operation and the type of the computing device (controller) used. The tool is powered at the 50 Hz and 400 Hz, and these are also the main interference frequencies.

Denote the filter cutoff frequency f_c, then the filter's bandwidth will be Δf_c. The bandwidth can be estimated using the approximating equation for FIR-filters (Smith, 1999):

$$\Delta f_c = 4 \cdot \frac{f_D}{M}. \quad (10)$$

It follows from this equation that the wider the kernel of filter M is, the narrower is the bandwidth. The sampling rate f_D in the numerator means that the growth of the filter kernel which can be achieved by creating more samples over the observation time will in practice cause the bandwidth Δf_c to remain unchanged. Therefore, the only way to significantly narrow the bandwidth is to increase the observation time, which in turn is limited by the speed of logging.

Denote by $h[i]$ the impulse response of the FIR-filter. As known (Smith, 1999; Ifeachor and Jervis, 2001), the construction of the FIR-filter (finding all the coefficients of $h[i]$) can be determined by overlapping the truncated sinc-function to any of the known weight functions:

$$h[i] = K \cdot \frac{\sin\left(2\pi f_c\left(i - \frac{M}{2}\right)\right)}{i - \frac{M}{2}} \cdot w(i).$$

In equation (11) $w(i)$ is a weight function. The cutoff frequency f_c, expressed as a fraction of the sample rate, varies from 0 to 0.5. The length of the filter kernel is determined by the value M, which must be an even integer. The data index i is an integer varying from 0 to M, which gives $M + 1$ points into the kernel. The constant K is selected from the condition for obtaining a unit gain at zero frequency. To avoid division by zero, we take $h[i] = 2\pi f_c K$ for $i = M/2$. In the sinc-function, the independent variable i is shifted $M/2$ points to the right in the time domain in order to avoid a negative index.

As a weight function, various windows are usually used, for example, the Hamming window, the Blackman window, or others. This depends on the required parameters of the bandwidth, the suppression ratio, and the slope of the char-

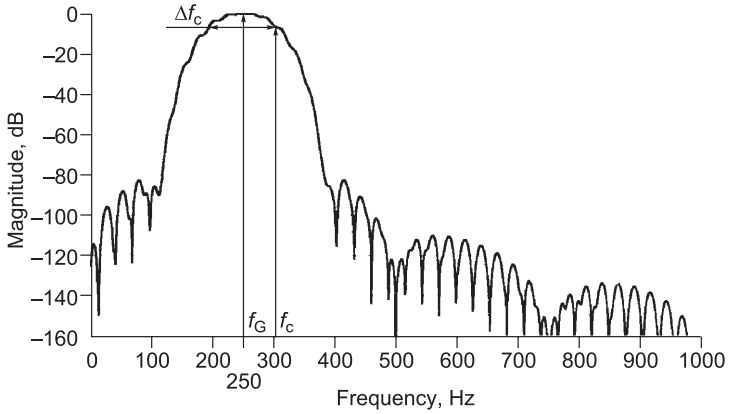

Fig. 3. The frequency response of the digital filter.

acteristic. For example, in 5LL, the Kaiser window was used as a weight function (Ifeachor and Jervis, 2001).

Figure 3 shows the final frequency response of both the FIR module and the DFT module, constructed for the selected weight function and the *M* kernel, which allowed this filtering to be implemented in real time. The resulting FIR-filter provided unevenness of no more than 0.2% in the band 248...252 Hz, and no more than 0.3% in the 245...255 Hz. Taking into account all the restrictions, the bandwidth is 55 Hz. In the stopband, the suppression ratio will be no worse than –83 dB. At a frequency close to 400 Hz, the suppression ratio will be no worse than –95 dB. Such a high suppression ratio at 400 Hz was obtained because of the relation (9) between the generated signal and the main frequency of the interference (the frequency of 400 Hz fell into the local minimum on the frequency response).

One of the requirements for digital filtration works in real time. This means that the microcontroller used during the time between two data samples must poll the ADC according to the existing protocol, transmit the received data to the FIR-filter, perform a convolution of the input sample with the FIR-filter kernel, and when the sample number is reached equal to the length of the FIR-filter kernel ($n = M$), perform a "run" of the newly calculated data through the DFT module. The main parameters that affect the calculation rate are the controller clock frequency, the controller type, the filter kernel length, and the sample rate.

Evaluating the capabilities of the DSP core, that is, determining the number of the commands spent on one of *M* iterations of the FIR-filter, as well as calculating the number of the commands spent on each program module during the time between two samples leads to the first equation for optimization:

$$f_D = \frac{f_T}{N_D}, \tag{12}$$

where f_T is the controller clock frequency, and N_D is the number of operations that the microcontroller must perform between two data samples (during t_D). The number of operations can be described as:

$$N_D = N_0 + N_{DFT} + N_{FIR}, \tag{13}$$

where N_0 is the number of general-purpose operations, N_{DFT} is the number of operations spent on calculating the DFT, N_{FIR} is the number of operations spent on FIR filtering. General N_0 operations include operations spent on working with the ADC, transferring data between variables, and commands for performing transitions between filter modules. The number of operations spent on the DFT (N_{DFT}) depends on the number of samples used. The number of operations spent on FIR filtering for a controller with a DSP core can be expressed through the filter kernel:

$$N_{FIR} = C \cdot M, \tag{14}$$

where *C* is the number of instructions (clock periods) for calculating one point. For example, to calculate a single point, a controller with a DSP core must execute 4 commands. In equation (14), the parameter *C* depends on the type of the controller used, so if one uses a controller without a DSP core, the number of instructions for calculating one filter point will increase.

The second optimization equation is derived based on the requirements of the correct operation of the DFT algorithm:

$$f_D = \frac{M \cdot f_G}{Q}, \tag{15}$$

where the parameter *Q* determines which part of the total samples of the signal *N* has a length *M* in the generation periods, it is recommended to determine it as an integer. By constructing graphs of the derived equations (12) and (15), it is possible to evaluate whether a particular controller can work with the given parameters in real time. Figure 4 shows graphs of these functions. The first optimization equation (12) determines the falling curve. This curve depends on the controller clock frequency and limits the area on the graph depending on the speed of the controller. The second opti-

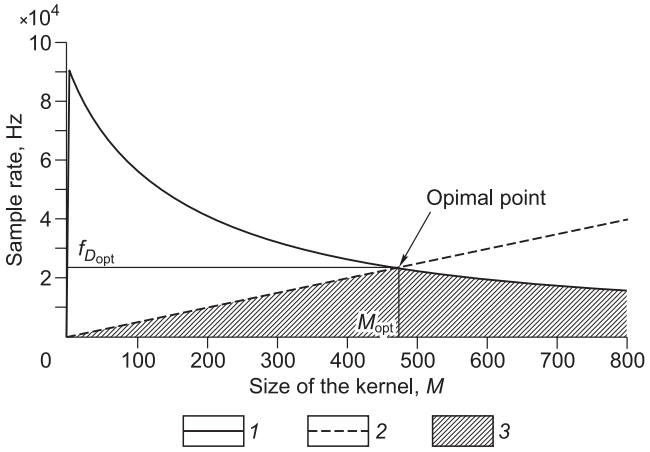

Fig. 4. Choosing the optimal point.

mization equation (15), for a given generation frequency f_G and parameter Q determines dependence of the size of the filter kernel M on the sampling rate f_D. According to equation (10), the more the size of the kernel and the higher the sampling rate are, the narrower the bandwidth Δf_C will be.

The purpose of constructing these graphs is the choice of the operating point, that is, the choice of the size of the filter kernel and the sampling frequency. It should be noted that the type of controller, its clock frequency, generation frequency and Q parameter is already considered selected. If the straight line in Fig. 4, which defines the second optimization equation, passes above the falling curve, then in this area the controller will not have time to execute a given number of commands. The shaded area defines the location where the operating point should be selected. If one selects the operating point under the dashed straight line and the solid curve, the resources will be used inefficiently – the controller will stand idle after all DSP operations until the next sample is received. In order to prevent this, one needs to select the operating point on the dashed line and the higher the better, since a narrower bandwidth Δf_C is provided in this case. However, an infinite increase in the operating point is not possible and is limited by the first optimization equation (12). The optimal point at which there will be no downtime of the controller and the narrowest bandwidth will be provided is at the intersection of the graphs. In Fig. 4, the optimal filter kernel size is denoted by M_{opt}, and the corresponding optimal sampling frequency f_{Dopt}. In real conditions, it is recommended to choose the optimal point just below the intersection, in order to obtain a guaranteed time for operations after each sample. The graphs in Fig. 4 are given with the following parameters: the generation frequency f_G was taken equal to 250 Hz, the controller clock frequency was taken equal to 60 MHz, the result of the sum $N_0 + N_{DFT}$ was taken equal to 700 commands, parameter Q was taken equal to 9. The number of commands spent on calculating one point C during filtering was set to 4. A similar digital filter calculated according to the method presented here, taking into account the optimal criteria for choosing the sampling frequency and the length of the filter kernel, was applied to all the measurement channels of the 5LL tool, but can also be applied to any resistivity tools (galvanic and induction).

THE WELL EXPERIMENTS

To analyze the results of applying the methods for increasing the dynamic range using the example of logging curves of the 5LL tool, we introduce the concept of the contrast. A contrast is the ratio of apparent resistivity (sonde reading) to mud resistivity. The readings of the laterolog sondes do not linearly depend on the resistivity of the formation, and with "sufficiently" high resistivity, a situation is observed where a small change in resistivity causes a large (infinite) change in the apparent resistivity. In this case, backward interpolation of the formation resistivity according to the readings of the tool becomes hardly possible, since it is not possible to evaluate which small change in the formation resistivity initially caused a large change in the readings of the tool. Contrast limits the value of the formation resistivity, which can be interpolated with the known mud resistivity.

The value of maximum contrast depends on:

– the ratio of the formation resistivity to the drilling mud resistivity;

– the sonde length: the longer the sonde, the greater the magnitude of the allowable contrast (less influence of the borehole effect);

– the ratio of the borehole diameter to the tool diameter: the smaller the difference between them, the greater the value of the allowable contrast;

– the tool position in the borehole (eccentricity).

One of these factors is the tool position in the borehole. The least restriction is observed when the tool is located on the borehole axis. When the tool approaches the borehole wall, the contrast does not significantly decrease for deep sondes, but for shallow ones, a nonlinear decrease of tens to hundreds of times is observed (the closer to the borehole wall, the less contrast). For example, for the 5LL tool, it was estimated that with a mud resistivity of 0.02 Ohm·m, the first shallow sonde (if it is on the borehole axis) is capable of distinguishing resistivity up to 400 Ohm·m with a borehole diameter 216 mm. Under the same conditions, when placed on a borehole wall, a shallow sonde can distinguish formation resistivity only up to 42 Ohm·m. Deep sondes (4th and 5th) under these conditions are not sensitive to the position of the tool (Klimenko et al., 2018).

Figure 5 shows an example of contrast limitation for the 1st and 2nd sonde of the 5LL tool according to the logging data in one of the wells in the Irkutsk region. Logging of the tool was carried out as part of pilot production, without installing centralizers; the tool was on the borehole wall. The well conditions: borehole diameter 216 mm, mud resistivity 0.02 Ohm·m. On the left, on the first track, primary, un-

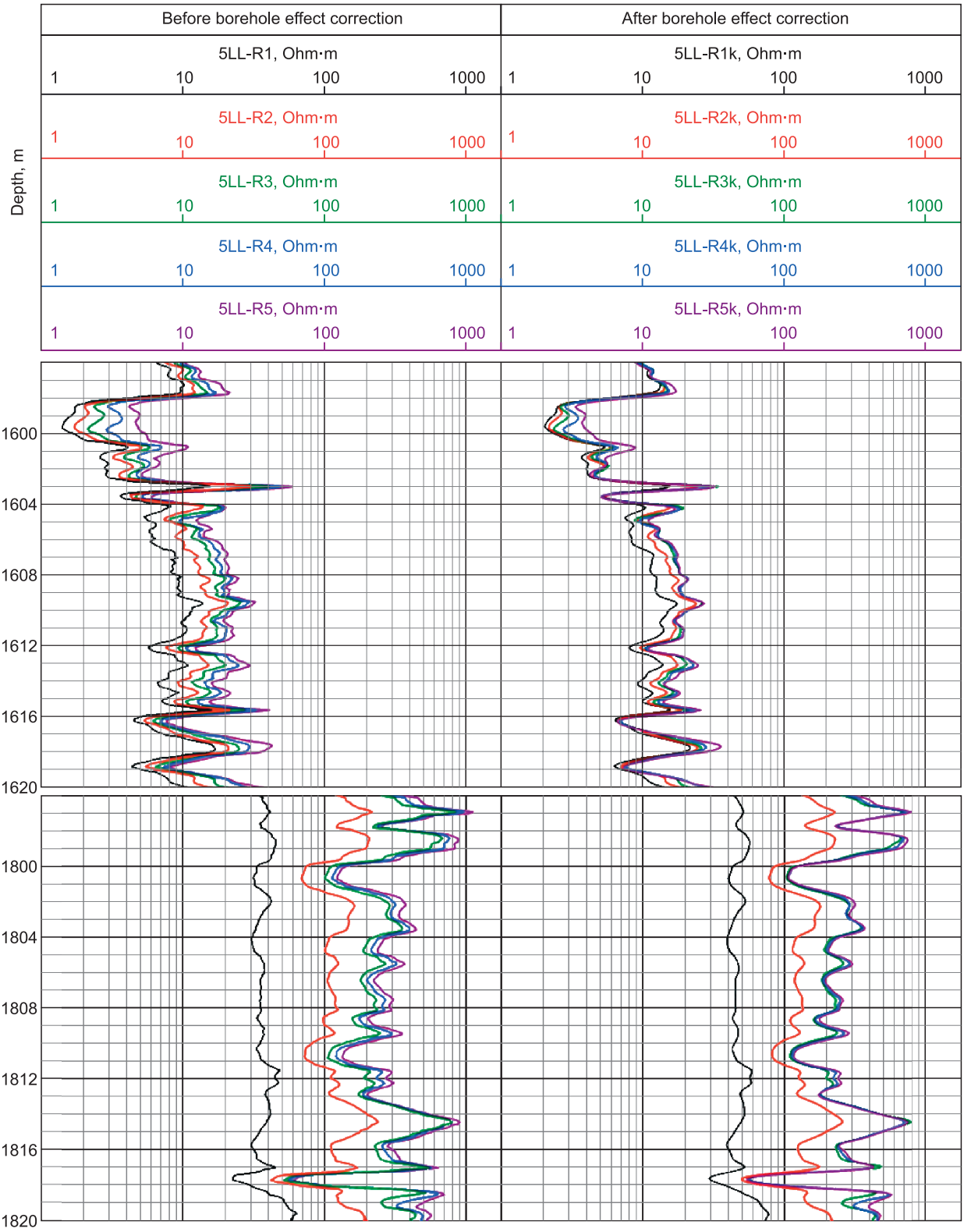

Fig. 5. Contrast restrictions for shallow sondes.

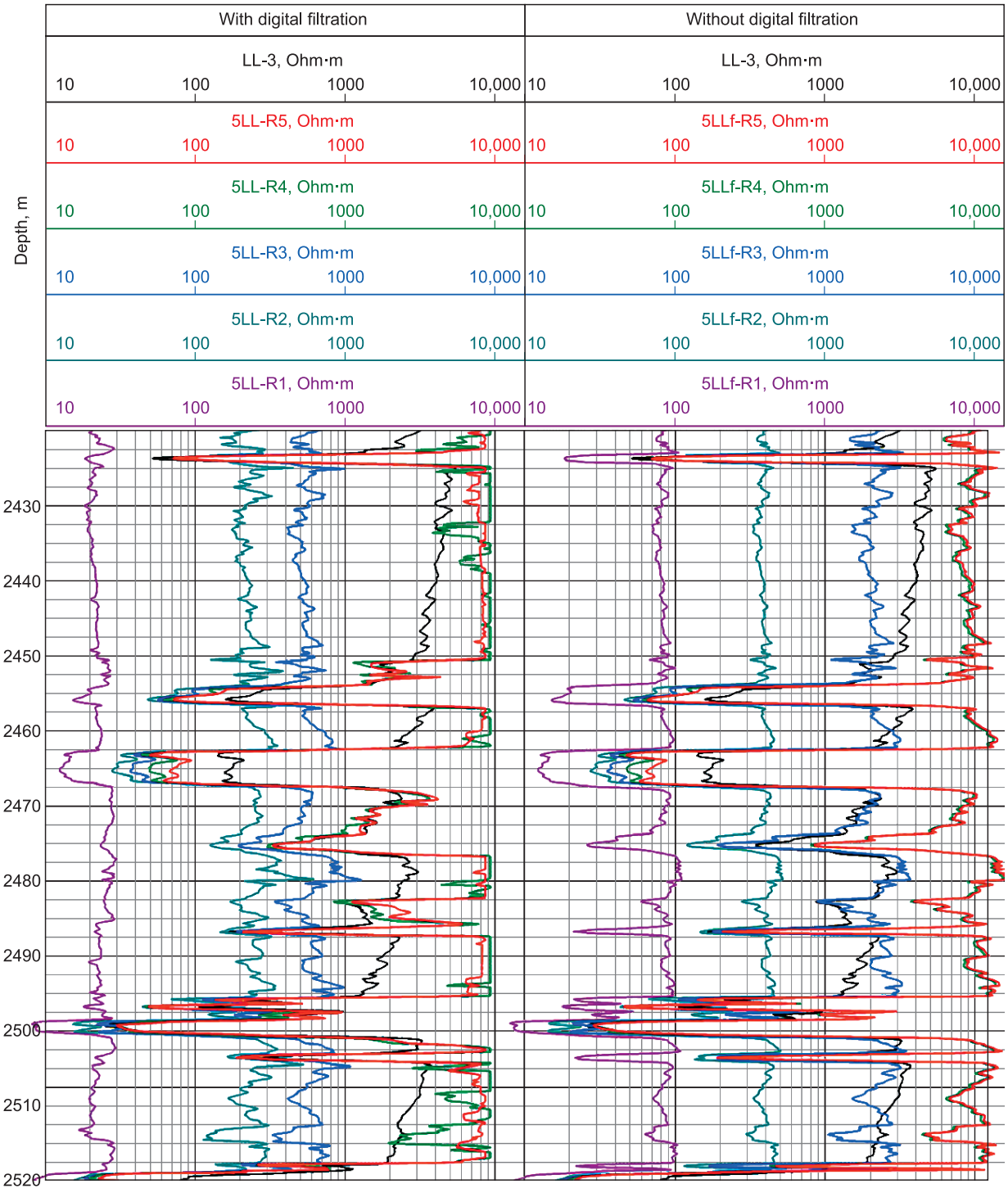

Fig. 6. Resistivity curves of tools LL3 and 5LL, Irkutsk region.

treated logging curves are shown; on the right, there are the same curves after corrections for the borehole effect and the tool eccentricity. Corrections for the borehole effect and the tool eccentricity are introduced classically (using charts), without any inversion.

In the upper interval of depths of 1596–1620 m, in layers with low resistivity, all the sondes of the 5LL tool work correctly. In the lower interval of depths of 1796–1820 m, contrasting saturation of the curves of the 1st and 2nd sonde (curves *5LL-R1a* and *5LL-R2a*, respectively) is observed, they degenerate into straight lines ("sticks"). Basically, these contrast limitations affect shallow sondes and mainly in high resistivity intervals.

For example, Fig. 6 shows the curves of the apparent resistivity of the LL3 and 5LL tools (corrected for the borehole effect), according to the initial logging data in the Ir-

kutsk region. On the left there are the apparent resistivity curves of the 5LL tool without using digital filtration (raw data with averaging), on the right – after using digital filtration. The hardware-based methods for increasing the dynamic range and mathematical focusing were used both on the left and on the right in the figure. The resistivity curve of the LL3 tool was also added to both tracks for comparison. Downhole conditions: the nominal borehole diameter 219 mm, mud resistivity 0.06–0.07 Ohm·m. Logging was carried out without the use of special centralizers or standoffs. The zenith angle of the well was about 20° in the given depth interval. Therefore, the tool was located on the wall during well logging. All curves are corrected for the borehole effect and the tool eccentricity.

On the left track in layers with high resistivity (more than 1000 Ohm·m), the curves of the 5LL tool deep sondes (4th *5LL-R4* and 5th *5LL-R5*) lie above the *LL3* curve, which is explained by the wider dynamic range (using mathematical focusing and hardware methods to increase the dynamic range). Due to the high contrast of the medium, the curves of the 1st (*5LL-R1*), 2nd (*5BK-R2*), 3rd (*5BK-R3*) sondes decomposed in accordance with their measurement limit and operate in these layers at the level of the intrinsic noise. The curves of the 4th and 5th sondes also entered contrast saturation, which is about 10,000 Ohm·m for these well conditions. This is noticeable in the behavior of the curve of the 4th sonde, which records above the 5th sonde in high-resistivity layers, that is, the measuring voltages of the 4th sonde are less noisy compared to the 5th sonde. If we assume that after the borehole effect correction the curves of the 5LL tool deep sondes opposite the impermeable layers read approximately formation resistivity, which is about 10,000 Ohm·m, then the ratio of formation resistivity to mud resistivity will amount to 140,000 ... 160,000 units. In the depth intervals: 2416.5–2423.4; 2424.5–2450.5; 2456.5–2462.5; 2476.5–2482.5; 2487–2495.5; 2505–2517.5 m opposite dense, geologically homogeneous formations, the LL3 curve enters saturation in contrast at the level of 3000…4000 Ohm·m, which ensures the ratio of formation resistivity to mud resistivity at 50,000…60,000 units. Satisfactory operation for the LL3 tool is maintained at a ratio of 40,000 or less and depends on the specific tool. After applying digital filtration (right track), the curves of the 4th (*5LLf-R4*) and 5th (*5LLf-R5*) sondes of the 5LL tool, in dense high-resistivity formations begin to draw formation resistivity, compared with the tendency to the straight line ("stick") on the left track. The curves of the 1st (*5LLf-R1*), 2nd (*5LLf-R2*), 3rd (*5LLf-R3*) sondes rose, digital filtration raised their measuring limit, the noise level for measuring voltages and currents became lower, but the resistivity curves still did not reach the value shown by deep sondes. The resistivity curve of the shallowest sonde (*5LLf-R1*), after using digital filtration, began to differentiate the formation cut; without filtration, this curve (*5LL-R1*) degenerates into a straight line. In low-resistivity well intervals, the use of digital filtration practically does not change the behavior of the curves, since the signal level in these layers is high (the signal-to-noise ratio is low).

Figure 7 shows the logging curves of the 5LL tools (digital filtration applied) at one of the fields in the Orenburg region. Downhole conditions: the nominal borehole diameter 219 mm, mud resistivity 0.18 Ohm·m, zenith angle of the well was about 25° in the study interval. Logging was carried out without the use of special centralizers or standoffs, the 5LL tool was located on the borehole wall. All the curves are corrected for the borehole effect and the tool eccentricity. In the depth intervals 2757–2772; 2773–2777.5; 2781–2783.5 m opposite the dense, high-resistivity, geologically homogeneous formations the curves *5LLf-R3*, *5LLf-R4*, *5LLf-R5* of the 5LL tool record much higher resistance than the 3LL tool curve (for example, approximately 12,000 Ohm·m opposite 6600 Ohm·m at the interval 2757–2772 m). Curves *5LLf-R1*, *5LLf-R2* in these layers enter to the saturation for these well conditions. Both tools worked correctly because in the depth interval 3580.5–3600 m (low electrical resistivity of the reservoir with a resistive invasion effect) the curves *LL3* and *5LLf-R5* coincide within the measurement error.

It should be noted that the LL33 curve in dense high-resistivity formations has a characteristic slope (in Fig. 6 and 7), which is consistent with the simulation results given in (Knizhnerman et al., 2013) and is explained by non-symmetry of the sonde and the position of the remote and current-return electrodes. In the depth interval 2463–2467 m (Fig. 6), due to the shield effect, the removed electrode potential changes and as a result, unnatural apparent resistivity overstatement is observed on the *LL3* curve below the high-resistivity layer. 5LL curves are much less prone to tilts and level distortion, since the tool remote electrodes are located symmetrically above and below, thereby ensuring equalization of potential.

CONCLUSIONS

In the experience of foreign companies, one of the approaches to struggle against high contrast (a strong borehole effect) is the adaptive borehole correction, proposed in (Zhou et al., 2008; Mauer et al., 2009). With this approach, the response of the tool in the well with "real" mud resistivity is replaced by the response with "virtual" mud resistivity equal to invasion zone resistivity in permeable or formation resistivity in impermeable layers (which are obtained from readings of deep sondes). This allows us to correct the readings of shallow sondes, including determination of the tool eccentricity, which is considered unknown. The algorithm is based on pointwise one-dimensional inversion without taking into account the influence of adjacent formations, which is performed during logging at a workstation on the surface, according to pre-calculated tables (charts). Similar inversion algorithms are used not only for laterolog tools, for example (Khusid, 2017; Mikhailov et al., 2017; Loginov and Petrov,

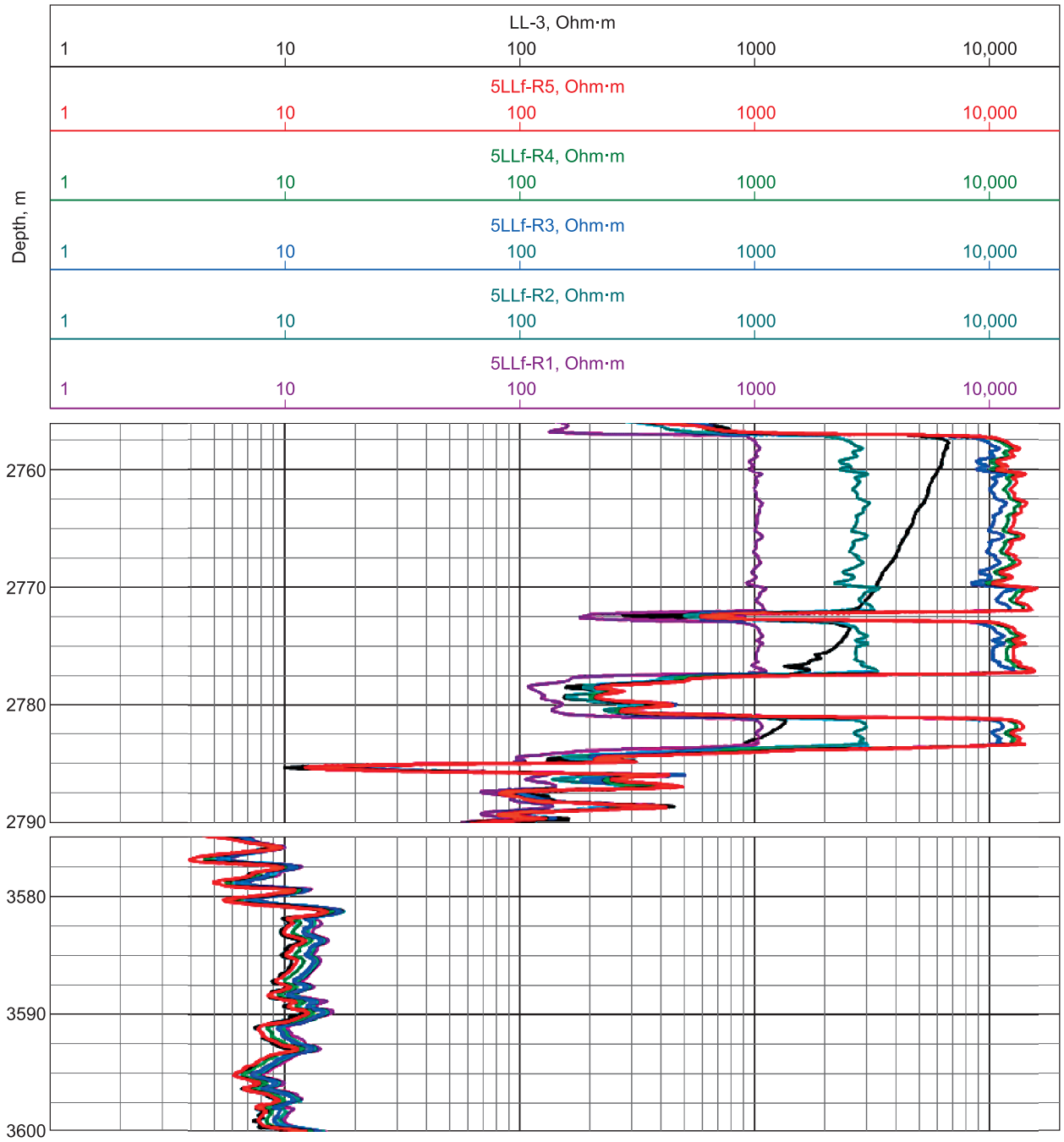

Fig. 7. Logging results, Orenburg region.

2019). However, the use of these approaches does not exclude the requirements for obtaining non-noisy data from the tool itself. The methods for obtaining non-noisy data are given in this article and they can be applied to any logging tool that uses generation of current of a certain frequency and subsequent signal selection with the same frequency.

Summarizing, we note that in order to extend the dynamic range for laterolog tools, the following conditions must be fulfilled:

– mathematical focusing;
– digital filtration;
– satisfaction of limitations of the ADC bit depth;
– satisfaction of requirements at the hardware level.

These conditions must be fulfilled jointly, failure to fulfill one of the conditions leads to futility of others and the impossibility of extending the dynamic range of the tool as a whole.

Further extension of the dynamic range is possible with using adaptive correction techniques for the borehole effect (one-dimensional pointwise inversion during logging) similarly to the best Western practices.

REFERENCES

Dakhnov, V.N., 1981. Electrical and magnetic methods of well research [in Russian]. Nedra, Moscow.

Gusev, V.G., Gusev, Yu.M., 2013. Electronics and microprocessor technology [in Russian]. KnoRus, Moscow.

Ifeachor, E.C., Jerwis, B.W., 2001. Digital signal processing: A practical approach. 2nd edition, Prentice Hall.

Il'inskii, V.M., 1971. Laterolog [in Russian]. Nedra, Moscow.

Itskovich, G.B., Mezzatesta, A.G., Strack, K.-M., Tabarovsky, L.A., 1998. High-definition lateral log – resistivity device: basic physics and resolution, in: SPWLA 39th Annual Logging Symposium: Conference paper (Keystone, Colorado, USA, 26–28 May 1998). https://www.onepetro.org/conference-paper/SPWLA-1998-V.

Kayazkas, A.A., 1988. Basics of radio-electronics [in Russian]. Vysshaya Shkola, Moscow.

Kayurov, K.N., Eremin, V.N., Petrov, A.N., Suhorukova, K.V., Nikitenko, M.N., Arzhantsev, V.S., 2015. SCL hardware tools systems for logging in oil-gas wells and its interpretation base. Neftyanoe Khozyaistvo, No. 9, 38–43.

Khusid, M.D., Kashik, M.D., Knizhnerman, L.A., 2014. Optimizing the electrologging and electro-thermal effects in cased wells via the transformations of the column's construction. Geofizika, No. 4, 69–73.

Khusid, M.D., Knizhnerman, L.A., Dyakonova, T.F., 2017. Application of the consecutive lateral correction method to the solution of the axisymmetric inverse problem of electrical and induction logging in geological areas with diagonally-anisotropic beds. Geofizika, Special Issue, 118–125.

Klaassen, K.B., 1996. Electronic measurement and instrumentation. Cambridge University Press.

Klimenko, V.A., Korovin, V.M., Salahov, T.R., 2018. Evaluation method of the mud resistivity according to multizonde laterolog curves. Neftegazovoe Delo, No.16 (5), 6–13.

Klimenko, V.A., Salahov, T.R., Shakirov, D.R., Popov, A.A., 2019. Russian multisonde laterolog tool for reservoir determination and estimation of oil saturation. Neftyanoe Khozyaistvo, No. 11, 88–93.

Legendre, E., Dubourg, I., Dobuy, J., Smits, J.W., Faivre, O., Griffiths, R., 1999. Better saturation from new array laterolog, in: SPWLA 40th Annual Logging Symposium: Conference paper (Oslo, Norway, 30 May – 3 June 1999, https://www.onepetro.org/conference-paper/SPWLA-1999-DDD.

Loginov, G.N., Petrov, A.M., 2019. Automatic detection of geoelectric boundaries according to lateral logging sounding data by applying a deep convolutional neural network. Russian Geology and Geophysics (Geologiya i Geofizika) 60 (11), 1319–1325 (1650–1657).

Maurer, H., Antonov, Y., Corley, B., Khokhar, R., Rabinovich, M., Zhou, Z., 2009. Advanced processing for a new array laterolog tool, in: SPWLA 50th Annual Logging Symposium: Conference paper (Woodlands, Texas, USA, 21–24 May 2009). https://www.onepetro.org/conference-paper/SPWLA-2009-56708.

Mikhailov, I.V., Glinskikh,V.N., Nikitenko, M.N., Surodina I.V., 2017. Joint inversion of induction and galvanic logging data in axisymmetric geological models. Russian Geology and Geophysics (Geologiya i Geofizika) 58 (6), 752–762 (935–947).

Salnikova, O.L., Savich, A.D., Chukhlov, A.S., 2019. An experience of applying the method of multisonde lateral logging. Karotazhnik, No. 5 (299), 55–61.

Smith, S.W., 1999. The Scientist and Engineer's Guide to Digital Signal Processing. California Technical Publishing, San Diego.

Smits, J.W., Dubourg, I., Luling, M.G., Minerbo, G.N., Koelman, J.M. V.A., Hoffman, L.J.B., Lomas, A.T., Oosten, R.K.v.d., Schiet, M.J., Dennis, R.N., 1998. Improved resistivity interpretation utilizing a new array laterolog tool and associated inversion processing, in: SPE Annual Technical Conference and Exhibition: Conference paper (New Orleans, Louisiana, USA, 27–30 September 1998). https://doi.org/10.2118/49328-MS.

Zhou, Z., Corley, B.H., Khokhar, R., Maurer, H.-M., Rabinovich, M., 2008. Adaptive borehole corrections accounting for eccentricity for array laterologs, in: SPE Annual Technical Conference and Exhibition: Conference paper (Denver, Colorado, USA, 21–24 September 2008). https://doi.org/10.2118/114704-MS.

Editorial responsibility: I.N. Yeltsov